The 2009 IEEE/RSJ International Conference on
Intelligent Robots and Systems
October 11-15, 2009 St. Louis, USA

Coordination Control of a Free-Flying Manipulator and Its Base Attitude to Capture and Detumble a Noncooperative Satellite

Farhad Aghili

Abstract— **This paper focuses on the guidance of a robot manipulator to capture a tumbling satellite and then bring it to state of rest (detumbling). First, a coordination control for combined system of the space robot and the target satellite, which acts as the manipulator payload, is presented so that the robot tracks the optimal path while regulating the attitude of the chase vehicle to a desired value. Subsequently, two optimal trajectories for the pre- and post-capture phases are designed. In the pre-capturing phase, the manipulator maneuvers are optimized by minimizing a cost function which includes the time of travel and the weighted norms of the end-effector velocity and acceleration, subject to the constraint that the robot end-effector and a grapple fixture on the satellite arrive at the rendezvous point with the same velocity. In the post-grasping phase, the manipulator dumps the initial velocity of the tumbling satellite in minimum time subject to the constraint that the magnitude of the torque applied to the satellite remains below a safe value. Simulation and experimental results are appended.**

I. Introduction

The control system of a space manipulator for on-orbit servicing of satellites usually requires two mode of operations: capturing and detumbling [1]–[3]. In the pre-capture phase, the manipulator arm is guided (typically with using vision data) so as its end-effector intercepts the satellite grapple fixture at a rendezvous point along the trajectory of the tumbling satellite. The capture will be without impact, if the manipulator approaches the target in such a manner that, at the time of capture, the relative velocity between the end-effector and the target grapple point is zero [4]. Otherwise, the effect of impact and on a free-floating space robot has to be taken into account [5]; an optimal trajectory planning to minimize the impulse during contact between two bodies was presented in [6]. After capture of an uncontrolled tumbling satellite by a space manipulator, the satellite should be brought to rest [7], [8]. To accomplish this goal, the space manipulator should gently apply torques to the target satellite for removing any relative velocity, ideally as fast as possible. In this paper, we are dealing with problems occurring in both pre- and post-capture of a tumbling satellite.

There are many studies on optimal trajectory planning to guide a robotic manipulator to rendezvous and capture a non-cooperative target satellite [9]–[12]. In the case that the target satellite dynamics is uncertain, not only the states but also the target's inertial parameters and its position of center of mass can be estimated from vision data obtained from zero motion of a tumbling satellite [12], [13]. However, there are only few studies on the path planning for detumbling of a non-cooperative satellite and non of which is optimal. In [14], the principle of conservation of momentum was used to damp out the chaser-target relative motion. However, there was no control on the force and moment built up at the connection of the chaser manipulator and the target. Impedance control scheme for a free-floating space robot in grasping of a tumbling target with model uncertainty is presented in [15], however optimal path planning is not addressed in this work.

The magnitude of the interaction torque between the space manipulator and the target must be constrained during the detumbling operation for two main reasons: First, too much interaction torque could cause mechanical damage to either the target satellite or to the space manipulator. Second, a large interaction torque may lead to actuation saturation of the space robot's attitude control system. This is because, the reaction of the torque on the space robot base should be eventually compensated for through additional momentum generated by the actuator of its attitude control system, e.g., momentum/reaction wheels, in order to keep the attitude of the base undisturbed. Moreover, it is important to dump the initial velocity of the target as quickly as possible in order to mitigate the risk of collision due to small but nonzero translational drifts of the satellites. Hence, optimal planning of the passivation maneuvers is highly desired [16].

This paper is organized as follow: Section II describes a coordination control for the combined system of the space robot and the target satellite so that the manipulator tracks a prescribed motion trajectory while regulating the attitude of its own base to a desired value. Optimal trajectory for robotic capturing of a tumbling satellite is presented in Section III. Section IV presents a closed-form solution for time-optimal detumbling maneuvers of a rigid spacecraft under the constraint that the Euclidean norm of the braking torques is below a prescribed value. Finally, experimental and simulation results are shown in Section V.

II. Control of the Combined System of Manipulator and Target

Fig. 1 illustrates the pre- and post-capture phases of an on-orbit servicing operation. In the post-capture phase, the space robot and the target satellite constitutes a single free-flying multibody chain. The dynamic equations of the space robot can be expressed in the form [1]

$$\boldsymbol{M}_s\ddot{\boldsymbol{\psi}}_s + \boldsymbol{c}_s(\boldsymbol{\psi}_s, \dot{\boldsymbol{\psi}}_s) = \boldsymbol{u} + \boldsymbol{J}^T\boldsymbol{f}_h, \tag{1}$$

F. Aghili is with the Spacecraft Engineering Division of the Space Technologies, Canadian Space Agency, Saint-Hubert, Quebec J3Y 8Y9, Canada farhad.aghili@space.gc.ca

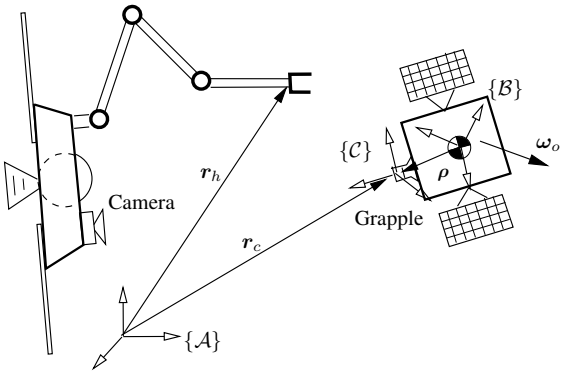

(a) Pre-contact phase

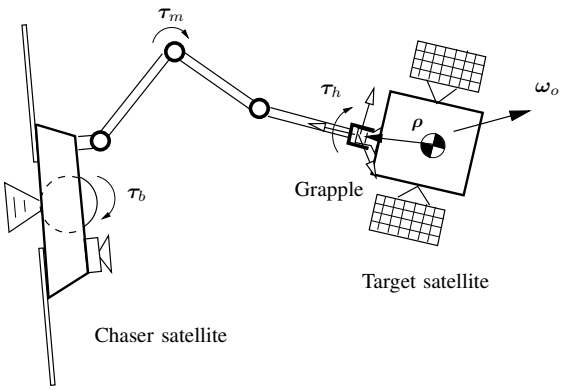

(b) Post-contact phase

Fig. 1. The free body diagram of chaser and target satellites

where

$$\dot{\psi}_s = \begin{bmatrix} \boldsymbol{\nu}_b \\ \dot{\boldsymbol{\theta}} \end{bmatrix}, \qquad \boldsymbol{u} = \begin{bmatrix} \boldsymbol{f}_b \\ \boldsymbol{\tau}_m \end{bmatrix}.$$

Here, $\boldsymbol{M}_s$ is the generalized mass matrix of the space manipulator, $\boldsymbol{c}_s$ is generalized Coriolis and centrifugal force, $\boldsymbol{\nu}_b^T = [\boldsymbol{v}_b^T \;\; \boldsymbol{\omega}_b^T]$ is the generalized velocity of the base consisting of the linear and angular velocities, $\boldsymbol{v}_b$ and $\boldsymbol{\omega}_b$, vector $\dot{\boldsymbol{\theta}}$ is the motion rate of the manipulator joint, vector $\boldsymbol{f}_h$ is the force and moment exerted by the manipulator hand, vector $\boldsymbol{f}_b$ is the force and moment exert on the centroid of the base, vector $\boldsymbol{\tau}_m$ is the manipulator joint torque and $\boldsymbol{J}$ is the Jacobian, which takes this form

$$\boldsymbol{J} = \begin{bmatrix} \boldsymbol{J}_b & \boldsymbol{J}_m \end{bmatrix}$$

with $\boldsymbol{J}_b$ and $\boldsymbol{J}_m$ being the Jacobian matrices for the base and for the manipulator arm, respectively. On the other hand, if the target spacecraft is rigid body, then its dynamics motion can be described by

$$\boldsymbol{M}_o \dot{\boldsymbol{\nu}}_o + \boldsymbol{c}_o = -\boldsymbol{A}^T \boldsymbol{f}_h \tag{2}$$

where $\boldsymbol{\nu}_o$ is the six-dimensional generalized velocity vector consisting of the velocity of the center of mass, $\boldsymbol{v}_o$, and the angular velocity, $\boldsymbol{\omega}_o$, components, $\boldsymbol{M}_o$ is the generalized mass matrix that can be written as

$$\begin{bmatrix} m\mathbf{1}_3 & \mathbf{0} \\ \mathbf{0} & \boldsymbol{I}_c \end{bmatrix} \quad \text{and} \quad \boldsymbol{c}_o = \begin{bmatrix} m\boldsymbol{\omega}_o \times \boldsymbol{v}_o \\ \boldsymbol{\omega}_o \times \boldsymbol{I}_c \boldsymbol{\omega}_o \end{bmatrix}$$

with m and $\boldsymbol{I}_c$ being the mass and the inertia tensor of the target satellite, and $\boldsymbol{A}$ can be expressed as

$$\boldsymbol{A} = \begin{bmatrix} \mathbf{1}_3 & \boldsymbol{\rho}\times \\ \mathbf{0} & \mathbf{1}_3 \end{bmatrix}$$

with $\boldsymbol{\rho}$ being the position vector of the target-spacecraft contact point with respect to its center of mass. Note that the RHS of (2) is the force and moment exert on the centroid of the target spacecraft. Furthermore, the generalized velocities of the manipulator hand and the target spacecraft are related by the following

$$\boldsymbol{\nu}_o = \boldsymbol{A}\boldsymbol{\nu}_h. \tag{3}$$

The velocity of the manipulator end-effector in the end-effector frame is expressed as

$$\boldsymbol{\nu}_h = \boldsymbol{J}\dot{\psi}_s = \boldsymbol{J}_b\boldsymbol{\nu}_b + \boldsymbol{J}_m\dot{\boldsymbol{\theta}} \tag{4}$$

The time-derivative of (4) leads to

$$\ddot{\boldsymbol{\theta}} = \boldsymbol{J}_m^{-1}\dot{\boldsymbol{\nu}}_h - \boldsymbol{J}_m^{-1}\boldsymbol{J}_b\dot{\boldsymbol{\nu}}_b - \boldsymbol{J}_m^{-1}(\dot{\boldsymbol{J}}_m\dot{\boldsymbol{\theta}} + \dot{\boldsymbol{J}}_b\boldsymbol{\nu}_b). \tag{5}$$

Now we are interested in writing the equations of motion in terms of the generalized velocities of the bases of the chaser and target satellites, i.e., $\boldsymbol{\nu}_b$ and $\boldsymbol{\nu}_h$. To this end, we define a new velocity vector as

$$\dot{\psi} \triangleq \begin{bmatrix} \boldsymbol{\nu}_b \\ \boldsymbol{\nu}_h \end{bmatrix} \tag{6}$$

The internal force vector $\boldsymbol{f}_h$ can be eliminated from (1) and (2) to yield the following equation

$$\boldsymbol{M}_s\ddot{\psi}_s + \boldsymbol{J}^T\boldsymbol{A}^{-T}\boldsymbol{M}_o\boldsymbol{A}\dot{\boldsymbol{\nu}}_h + \boldsymbol{J}^T\boldsymbol{A}^{-T}\boldsymbol{c}_o + \boldsymbol{c}_s = \boldsymbol{u} \tag{7}$$

Upon substitution of $\ddot{\boldsymbol{\theta}}$ from (5) into the corresponding component of $\ddot{\psi}_s$ in (7) the latter equation can be written in this form

$$\boldsymbol{M}\ddot{\psi} + \boldsymbol{c}(\psi, \dot{\psi}) = \boldsymbol{u}, \tag{8}$$

where

$$\boldsymbol{M} \triangleq \boldsymbol{M}_s \begin{bmatrix} \mathbf{1} & \mathbf{0} \\ -\boldsymbol{J}_m^{-1}\boldsymbol{J}_b & \boldsymbol{J}_m^{-1} \end{bmatrix} + \begin{bmatrix} \mathbf{0} & \boldsymbol{J}^T\boldsymbol{A}^{-T}\boldsymbol{M}_o\boldsymbol{A} \end{bmatrix}$$

$$\boldsymbol{c} \triangleq \boldsymbol{M}_s \begin{bmatrix} \mathbf{0} \\ -\boldsymbol{J}_m^{-1}(\dot{\boldsymbol{J}}_m\dot{\boldsymbol{\theta}} + \dot{\boldsymbol{J}}_b\boldsymbol{\nu}_b) \end{bmatrix} + \boldsymbol{J}^T\boldsymbol{A}^{-T}\boldsymbol{c}_o + \boldsymbol{c}_s,$$

in which we used the expression of the joint acceleration from (5). Note that (8) describes the dynamic motion of the combined chaser and target satellites in terms of their base variables. The special case of interest is when no force is applied to the base of the chaser satellite. In other words, the joint motion of the manipulator arm is allowed to disturb the base translation but not its attitude. Form a practical point of view, it is important to keep the base attitude unchanged as the spacecraft has to always point its antenna toward the Earth, whereas disturbing the base translation does not pose any significant side effect. Therefore, the generalized force input $\boldsymbol{u}$ consists of a 3×1 zero vector plus the vectors of the chaser base torque and the manipulator joint torque, i.e.,

$$\boldsymbol{u} = \begin{bmatrix} \mathbf{0}_{3\times 1} \\ \bar{\boldsymbol{\tau}} \end{bmatrix} \quad \text{where} \quad \bar{\boldsymbol{\tau}} \triangleq \begin{bmatrix} \boldsymbol{\tau}_b \\ \boldsymbol{\tau}_m \end{bmatrix}. \tag{9}$$

In view of the zero components of input vector (9), we will derive the reduced form of the equation of motion (8) in the following. Let us assume that

$$\dot{\boldsymbol{\psi}} \triangleq \begin{bmatrix} \boldsymbol{v}_b \\ \dot{\bar{\boldsymbol{\psi}}} \end{bmatrix} \qquad \text{where} \qquad \dot{\bar{\boldsymbol{\psi}}} \triangleq \begin{bmatrix} \boldsymbol{\omega}_b \\ \boldsymbol{\nu}_h \end{bmatrix}$$

is the velocity components of interest. Also, assume that the mass matrix and the nonlinear vector in (8) are partitioned as

$$\boldsymbol{M} = \begin{bmatrix} \boldsymbol{M}_{11} & \boldsymbol{M}_{12} \\ \boldsymbol{M}_{12}^T & \boldsymbol{M}_{22} \end{bmatrix} \quad \text{and} \quad \boldsymbol{c} = \begin{bmatrix} \boldsymbol{c}_1 \\ \boldsymbol{c}_2 \end{bmatrix}, \tag{10}$$

so that $\boldsymbol{M}_{11} \in \mathbb{R}^{3\times 3}$, $\boldsymbol{c}_1 \in \mathbb{R}^3$ and the dimensions of rest of submatrices and subvectors are consistent. Then, matrix equation (8) can be divided into two equations as:

$$\boldsymbol{M}_{11}\dot{\boldsymbol{v}}_b + \boldsymbol{M}_{12}\dot{\bar{\boldsymbol{\psi}}} + \boldsymbol{c}_1 = \boldsymbol{0} \tag{11}$$

$$\bar{\boldsymbol{M}}\ddot{\bar{\boldsymbol{\psi}}} + \bar{\boldsymbol{c}} = \bar{\boldsymbol{\tau}}, \tag{12}$$

where $\bar{\boldsymbol{M}}$ and $\bar{\boldsymbol{c}}$ are constructed from (10) as

$$\begin{aligned} \bar{\boldsymbol{M}} &= \boldsymbol{M}_{22} - \boldsymbol{M}_{12}^T\boldsymbol{M}_{11}^{-1}\boldsymbol{M}_{12} \\ \bar{\boldsymbol{c}} &= \boldsymbol{c}_2 - \boldsymbol{M}_{12}\boldsymbol{M}_{11}^{-1}\boldsymbol{c}_1. \end{aligned}$$

Autonomous system (11) is the manifestation of the *conservation of linear momentum* and hence it should be integrable, i.e.,

$$\frac{\mathrm{d}}{\mathrm{dt}}\big(\boldsymbol{M}_{11}\boldsymbol{v}_b + \boldsymbol{M}_{12}\bar{\boldsymbol{\psi}}\big) = \boldsymbol{0} \tag{13}$$

which can be used to estimate the base linear velocity. Equation (12) shows that through torque control input $\bar{\boldsymbol{\tau}}$, it is possible to simultaneously control the pose of the target satellite and the attitude of the chaser satellite. Therefore, the objective is to develop a coordination controller which sends torque commands to motors of the manipulator joints and to actuators of the attitude control system, e.g., reaction/momentum wheels, in order to not only track the optimal trajectories, which will be discussed in the following sections, but also to regulate the base attitude. To achieve this goal, we use a feedback linearization method based on dynamic model (12). Suppose that orientation of the robot base and hand are represented by quaternions $\boldsymbol{q}_b$ and $\boldsymbol{q}_h$, respectively. Then adopting a simple PD quaternion feedback [17] for the spacecraft attitude control, an appropriate feedback linearization control torque is given by

$$\bar{\boldsymbol{\tau}} = \bar{\boldsymbol{\tau}}_{ff} - \bar{\boldsymbol{M}}\begin{bmatrix} \boldsymbol{K}_{bp}\mathrm{vec}(\delta\boldsymbol{q}_b) + \boldsymbol{K}_{bd}\boldsymbol{\omega}_b \\ \boldsymbol{K}_{hp}\mathrm{vec}(\delta\boldsymbol{q}_h) + \boldsymbol{K}_{hd}(\omega_h - \omega_h^*) \\ \boldsymbol{K}_{rp}(\boldsymbol{r}_h - \boldsymbol{r}_h^*) + \boldsymbol{K}_{rd}(\dot{\boldsymbol{r}}_h - \dot{\boldsymbol{r}}_h^*) \end{bmatrix} \tag{14}$$

where

$$\bar{\boldsymbol{\tau}}_{ff} = \bar{\boldsymbol{c}} + \bar{\boldsymbol{M}}\begin{bmatrix} \boldsymbol{0}_{3\times 1} \\ \dot{\boldsymbol{\nu}}_h^* \end{bmatrix}$$

is the feed forward term and all feedback gains are positive definite. In the above, and quaternion errors are defined as

$$\delta\boldsymbol{q} = \boldsymbol{q} \otimes \boldsymbol{q}^*$$

where $\mathrm{vec}(\cdot)$ returns the vector part or quaternion $(\cdot)$ and the quaternion product operator $\otimes$ is defined as

$$\boldsymbol{q}\otimes \triangleq \begin{bmatrix} q_s\boldsymbol{1}_3 - \boldsymbol{q}_v\times & \boldsymbol{q}_v \\ -\boldsymbol{q}_v^T & q_s \end{bmatrix},$$

where $\boldsymbol{q}_v$ and q_s are the vector and scalar parts of the quaternion $\boldsymbol{q} = \mathrm{col}\,(\boldsymbol{q}_v, q_s)$.

Note that $\dot{\boldsymbol{\nu}}_h^*$ and $\boldsymbol{\nu}_h^*$ are obtained from the trajectory generator as will be shown the next section. Now substituting the control law (14) into (12) results in a set of three uncoupled differential equations as

$$\dot{\boldsymbol{\omega}}_b + \boldsymbol{K}_{bd}\boldsymbol{\omega}_b + \boldsymbol{K}_{bp}\mathrm{vec}(\delta\boldsymbol{q}_b) = \boldsymbol{0} \tag{15a}$$

$$(\dot{\boldsymbol{\omega}}_h - \dot{\boldsymbol{\omega}}_h^*) + \boldsymbol{K}_{hd}(\boldsymbol{\omega}_h - \boldsymbol{\omega}_h^*) + \boldsymbol{K}_{hp}\mathrm{vec}(\delta\boldsymbol{q}_h) = \boldsymbol{0} \tag{15b}$$

$$(\ddot{\boldsymbol{r}}_h - \ddot{\boldsymbol{r}}_h^*) + \boldsymbol{K}_{rd}(\dot{\boldsymbol{r}}_h - \dot{\boldsymbol{r}}_h^*) + \boldsymbol{K}_{rp}(\boldsymbol{r}_h - \boldsymbol{r}_h^*) = \boldsymbol{0} \tag{15c}$$

The exponential stability of the system (15c) is obvious, while the stability proof of systems (15a) and (15b) is given in the following analysis.

The quaternion evolves in time according to the following differential equation

$$\dot{\boldsymbol{q}}_b = \frac{1}{2}\underline{\boldsymbol{\omega}}_b \otimes \boldsymbol{q}_b \qquad \text{where} \qquad \underline{\boldsymbol{\omega}}_b = \begin{bmatrix} \boldsymbol{\omega}_b \\ 0 \end{bmatrix}. \tag{16}$$

Now, we define the following positive-definite Lyapunov function:

$$V = \frac{1}{2}\delta\boldsymbol{q}_{b_v}^T\boldsymbol{K}_p\delta\boldsymbol{q}_{b_v} + \frac{1}{2}\|\boldsymbol{\omega}_b\|^2. \tag{17}$$

Then, it can be shown by substitution from the quaternion propagation equation (16) that time derivative of V along trajectory (15a) is

$$\dot{V} = -\boldsymbol{\omega}_b^T\boldsymbol{K}_d\boldsymbol{\omega}_b \tag{18}$$

so that $\dot{V} \leq 0$ for all t. Therefore, according to LaSalle's Global Invariant Set Theorem [18], [19], the equilibrium point reaches where $\dot{V} = 0$, or $\boldsymbol{\omega}_b \equiv \boldsymbol{0}$. Then, we have from (15a)

$$\boldsymbol{K}_p\mathrm{vec}(\delta\boldsymbol{q}_b) = 0.$$

On the other hand it is known that two coordinate systems coincides if, and only if, $\delta\boldsymbol{q}_b = 0$, where the $\delta\boldsymbol{q}_b$ is the vector component of the quaternion [17]. Therefore, we have global asymptotic convergence of the orientation error. The stability of (15b) can be proved similarly.

Therefore, we can say $\boldsymbol{r}_h \to \boldsymbol{r}_h^*$, $\boldsymbol{q}_h \to \boldsymbol{q}_h^*$ and $\boldsymbol{q}_b \to \boldsymbol{q}_b^*$ as $t \to \infty$. Note that the role of feedback gains in (14) is to compensate for a possible modelling uncertainty, otherwise a feed forward controller as $\bar{\boldsymbol{\tau}} = \bar{\boldsymbol{\tau}}_{ff}$ suffices to achieve the control objective.

III. Optimal Maneuvers for Pre-Capture Phase

A. Path Planning

Dynamics of the rotational motion of the target satellite can be expressed by Euler's equation as

$$\dot{\boldsymbol{\omega}}_o = \boldsymbol{\phi}(\boldsymbol{\omega}_o) + \boldsymbol{I}_c^{-1}\boldsymbol{\tau}_o \tag{19}$$

where $\phi(\boldsymbol{\omega}_o) \triangleq -\boldsymbol{I}_c^{-1}(\boldsymbol{\omega}_o \times \boldsymbol{I}_c\boldsymbol{\omega}_o)$. Similar to (16), the time-derivative of the quaternion $\boldsymbol{q}_o$ representing the attitude of the target satellite is described by

$$\dot{\boldsymbol{q}}_o = \frac{1}{2}\underline{\boldsymbol{\omega}}_o \otimes \boldsymbol{q}_o \tag{20}$$

In the pre-capture phase, no external torque or force is applied to the target satellite. Thus

$$\boldsymbol{\tau}_o = \boldsymbol{0} \qquad \text{and} \qquad \ddot{\boldsymbol{r}}_o = \boldsymbol{0}, \tag{21}$$

where $\boldsymbol{r}_o$ is the location of the center of mass of the target satellite. Assume that $\boldsymbol{x} = \operatorname{col}(\boldsymbol{q}_o, \boldsymbol{\omega}_o, \boldsymbol{r}_o, \dot{\boldsymbol{r}}_o)$ represent the states of the target satellite. Then, state equations (19), (20) and (21) can be written collectively in the following compact form

$$\dot{\boldsymbol{x}} = \boldsymbol{f}(\boldsymbol{x}) \tag{22}$$

A short-term prediction of the states can be obtained by integrating (22), i.e.,

$$\boldsymbol{x}(t) = \boldsymbol{x}(t_0) + \int_{t_0}^{t} \boldsymbol{f}(\boldsymbol{x})d\tau.$$

Now, denoting the position of the grapple fixture mounted on the target satellite with $\boldsymbol{r}_c$ and assuming that the vector is expressed in $\{\mathcal{A}\}$, we have

$$\boldsymbol{r}_c(\boldsymbol{x}) = \boldsymbol{r}_o + \boldsymbol{R}(\boldsymbol{q}_o)\boldsymbol{\rho}. \tag{23}$$

Here the rotation matrix $\boldsymbol{R}(\boldsymbol{q})$ from $\{\mathcal{B}\}$ to $\{\mathcal{A}\}$ can be obtained from the quaternion q as

$$\boldsymbol{R}(\boldsymbol{q}) = (2q_s^2 - 1)\boldsymbol{1}_4 + 2q_s[\boldsymbol{q}_v\times] + 2\boldsymbol{q}_v\boldsymbol{q}_v^T. \tag{24}$$

Furthermore, knowing that, in $\{\mathcal{B}\}$, $\dot{\boldsymbol{R}} = \boldsymbol{R}[\boldsymbol{\omega}_o\times]$, we can calculate the velocity $\dot{\boldsymbol{r}}_c$ from the states as:

$$\dot{\boldsymbol{r}}_c(\boldsymbol{x}) = \boldsymbol{R}(\boldsymbol{q})(\boldsymbol{\omega}_o \times \boldsymbol{\rho}). \tag{25}$$

Let us represent the position of the end-effector in $\{\mathcal{A}\}$ as $\boldsymbol{r}_h(t)$. The end-effector and the grasping point are expected to arrive at a rendezvous-point simultaneously with the same velocity. Therefore, our objective is to bring the end-effector from its initial position to a grasping location, i.e., $\boldsymbol{r}_h(t_{f_1}) = \boldsymbol{r}_c(t_{f_1})$ and $\dot{\boldsymbol{r}}_h(t_{f_1}) = \dot{\boldsymbol{r}}_c(t_{f_1})$, while satisfying some optimality criteria. Let's assume that the optimal trajectory is generated by

$$\ddot{\boldsymbol{r}}_h^* = \boldsymbol{v}. \tag{26}$$

Then, denoting the augmented states by $\boldsymbol{\chi} = \operatorname{col}(\boldsymbol{x}, \boldsymbol{r}_h, \dot{\boldsymbol{r}}_h)$ and combining the deterministic part of systems (22) and (26), we get the following autonomous system

$$\dot{\boldsymbol{\chi}}(\boldsymbol{\chi}, \boldsymbol{v}) = \begin{bmatrix} \boldsymbol{f}(\boldsymbol{x}) \\ \dot{\boldsymbol{r}}_h \\ \boldsymbol{v} \end{bmatrix}. \tag{27}$$

Here, an optimal solution to input $\boldsymbol{v}$ is sought to drive the robot from the initial position to the final position while minimizing the following performance index (PI)

$$J = \int_0^{t_{f_1}} \big(1 + w_1\|\dot{\boldsymbol{r}}_h\|^2 + w_2\|\boldsymbol{v}\|^2\big)d\tau, \tag{28}$$

with $w_1, w_2 > 0$ and the final time t_{f_1} free. Note that due to the term t_{f_1} arising from the integral, the interception must be accomplished within a short time period. Thus, if the weights w_1 and w_2 are selected to be small, the term t_{f_1} dominates the PI yielding a time-optimal solution. On the other hand, since weights w_1 and w_2 penalize the PI by the magnitudes of the velocity and the acceleration during the travel, the latter quantities can be minimized if the corresponding weights are selected with relatively large values. Now, consider plant (27) and the performance objective of minimizing (28) with the following terminal state constraints:

$$\boldsymbol{\psi}_1(\boldsymbol{\chi}(t_{f_1})) = 0 \quad \text{where} \quad \boldsymbol{\psi}_1(\chi) = \begin{bmatrix} \boldsymbol{r}_c(\boldsymbol{x}) - \boldsymbol{r}_h \\ \dot{\boldsymbol{r}}_c(\boldsymbol{x}) - \dot{\boldsymbol{r}}_h \end{bmatrix} \in \mathbb{R}^6. \tag{29}$$

In the following, we will solve the above design equations explicitly for the optimal input $\boldsymbol{v}(t)$. Splitting the vector of costates $\boldsymbol{\lambda}$ as $\boldsymbol{\lambda} = \operatorname{col}(\boldsymbol{\lambda}_s, \boldsymbol{\lambda}_m)$, where $\boldsymbol{\lambda}_s \in \mathbb{R}^{12}$ and $\boldsymbol{\lambda}_h = \operatorname{col}(\boldsymbol{\lambda}_{h_1}, \boldsymbol{\lambda}_{h_2})$ with $\boldsymbol{\lambda}_{h_1}, \boldsymbol{\lambda}_{h_2} \in \mathbb{R}^3$, we can write the Hamiltonian of the system (27) and (28) as

$$\begin{aligned}\mathcal{H}(\boldsymbol{\chi}, \boldsymbol{v}, \boldsymbol{\lambda}_1) = 1 + w_1\|\dot{\boldsymbol{r}}_h\|^2 + w_2\|\boldsymbol{v}\|^2 + \boldsymbol{\lambda}_s^T\boldsymbol{f}(\boldsymbol{x}) \\ + \boldsymbol{\lambda}_{h_1}^T\dot{\boldsymbol{r}}_h + \boldsymbol{\lambda}_{h_2}^T\boldsymbol{v}.\end{aligned} \tag{30}$$

Since the Hessian of the Hamiltonian is positive-definite, i.e., $\mathcal{H}_{uu} = 2w_2\boldsymbol{1}_3 > 0$, the sufficient condition for local minimality is satisfied. According to the optimal control theory [20], optimal costate, $\boldsymbol{\lambda}^*$, and the optimal input, $\boldsymbol{v}^*$, must satisfy the following partial derivatives:

$$\dot{\boldsymbol{\lambda}}_1 = -\frac{\partial\mathcal{H}_1}{\partial\boldsymbol{\chi}}, \qquad \frac{\partial\mathcal{H}_1}{\partial\boldsymbol{v}} = 0. \tag{31}$$

Applying (31) to our Hamiltonian (30), we obtain the equations of motion of the costate

$$\dot{\boldsymbol{\lambda}}_s = -(\frac{\partial\boldsymbol{f}}{\partial\boldsymbol{x}})^T\boldsymbol{\lambda}_s \tag{32a}$$

$$\dot{\boldsymbol{\lambda}}_{h_1} = \boldsymbol{0} \tag{32b}$$

$$\dot{\boldsymbol{\lambda}}_{h_2} = -2w_1\dot{\boldsymbol{r}}_h - \boldsymbol{\lambda}_{h_1}. \tag{32c}$$

and the optimal input

$$\boldsymbol{v} = \ddot{\boldsymbol{r}}_h = -\frac{\boldsymbol{\lambda}_{h_2}}{2w_2}. \tag{33}$$

Equation (32b) implies that $\boldsymbol{\lambda}_{h_1}$ is a constant vector, and hence it is eliminated from the time-derivative of (32c), i.e.,

$$\ddot{\boldsymbol{\lambda}}_{h_2} = -2w_1\ddot{\boldsymbol{r}}_h. \tag{34}$$

Therefore, substituting the acceleration from (33) into (34) gives

$$\ddot{\boldsymbol{\lambda}}_{h_2} - \sigma^2\boldsymbol{\lambda}_{h_2} = \boldsymbol{0}, \tag{35}$$

where $\sigma = \sqrt{w_1/w_2}$. Finally, from (33) and (35), we can obtain the differential equation of the optimal trajectory as

$$\frac{d^2}{dt^2}\big(\ddot{\boldsymbol{r}}_h - \sigma^2\boldsymbol{r}_h\big) = \boldsymbol{0}, \tag{36}$$

the solution of which takes the following form

$$\boldsymbol{r}_h^*(t) = \boldsymbol{\kappa}_0 + \boldsymbol{\kappa}_1 t_{f_1} + \boldsymbol{\kappa}_2 e^{\sigma t_{f_1}} + \boldsymbol{\kappa}_3 e^{-\sigma t_{f_1}}. \tag{37}$$

Coefficients $\boldsymbol{\kappa}_0, \boldsymbol{\kappa}_1, \boldsymbol{\kappa}_2, \boldsymbol{\kappa}_3 \in \mathbb{R}^3$ can be obtained by imposing the initial and terminal conditions (29). That is,

$$\begin{bmatrix} \mathbf{1}_3 & \mathbf{0} & \mathbf{1}_3 & \mathbf{1}_3 \\ \mathbf{0} & \mathbf{1}_3 & \sigma\mathbf{1}_3 & -\sigma\mathbf{1}_3 \\ \mathbf{1}_3 & t_{f_1}\mathbf{1}_3 & e^{\sigma t_{f_1}}\mathbf{1}_3 & e^{-\sigma t_{f_1}}\mathbf{1}_3 \\ \mathbf{0} & \mathbf{1}_3 & \sigma e^{\sigma t_{f_1}}\mathbf{1}_3 & -\sigma e^{\sigma t_{f_1}}\mathbf{1}_3 \end{bmatrix} \begin{bmatrix} \boldsymbol{\kappa}_0 \\ \boldsymbol{\kappa}_1 \\ \boldsymbol{\kappa}_2 \\ \boldsymbol{\kappa}_3 \end{bmatrix} = \begin{bmatrix} \boldsymbol{r}_h(0) \\ \dot{\boldsymbol{r}}_h(0) \\ \boldsymbol{r}_c(t_{f_1}) \\ \dot{\boldsymbol{r}}_c(t_{f_1}) \end{bmatrix}.$$

The above system has 12 independent equations with 12 unknowns, and hence a unique solution is expected.

B. Optimal Rendezvous Point

The *optimal Hamiltonian* $\mathcal{H}^* = \mathcal{H}(\boldsymbol{\chi}^*, \boldsymbol{v}^*, \boldsymbol{\lambda}^*)$ calculated at optimal point $\boldsymbol{v}^*$ and $\boldsymbol{\lambda}^*$ corresponding to (32) and (33) must satisfy $\mathcal{H}^*(t_{f_1}) = 0$, i.e.,

$$\begin{aligned} \mathcal{H}^*(t_{f_1}) = 1 &+ w_1\|\dot{\boldsymbol{r}}_h(t_{f_1})\|^2 - w_2\|\ddot{\boldsymbol{r}}_h(t_{f_1})\|^2 \\ &+ \boldsymbol{\lambda}_{h_1}^T\dot{\boldsymbol{r}}_h(t_{f_1}) + \boldsymbol{\lambda}_s^T(t_{f_1})\boldsymbol{f}(t_{f_1}) = 0. \end{aligned} \tag{38}$$

This gives the extra equation required to determine the optimal terminal time. The final values of the costate in (38) can be obtained from the end point constraint equation referred to as the *transversality* condition:

$$\boldsymbol{\lambda}(t_{f_1}) = \big(\frac{\partial \boldsymbol{\psi}_1}{\partial \boldsymbol{\chi}}\big)_{t_{f_1}}^T \boldsymbol{\alpha} \tag{39}$$

where $\boldsymbol{\alpha} \in \mathbb{R}^6$ is the Lagrangian multiplier owing to the constraint (29). Upon substituting equations (29), the transversality condition (39) yields

$$\begin{aligned} \boldsymbol{\alpha} &= -\boldsymbol{\lambda}_h(t_{f_1}) \\ \boldsymbol{\lambda}_s(t_{f_1}) &= -\big(\frac{\partial \boldsymbol{r}_c}{\partial \boldsymbol{x}}\big)_{t_{f_1}}^T \boldsymbol{\lambda}_{h_1} - \big(\frac{\partial \dot{\boldsymbol{r}}_c}{\partial \boldsymbol{x}}\big)_{t_{f_1}}^T \boldsymbol{\lambda}_{h_2}(t_{f_1}). \end{aligned} \tag{40}$$

Moreover, from the following identities

$$\dot{\boldsymbol{r}}_c = \frac{\partial \boldsymbol{r}_c}{\partial \boldsymbol{x}}\boldsymbol{f}(\boldsymbol{x}) \quad \text{and} \quad \ddot{\boldsymbol{r}}_c = \frac{\partial \dot{\boldsymbol{r}}_c}{\partial \boldsymbol{x}}\boldsymbol{f}(\boldsymbol{x}),$$

and (40), we obtain

$$\boldsymbol{\lambda}_s^T\boldsymbol{f}(t_{f_1}) = -\boldsymbol{\lambda}_{h_1}^T\dot{\boldsymbol{r}}_c(t_{f_1}) + 2w_2\ddot{\boldsymbol{r}}_h(t_{f_1})^T\ddot{\boldsymbol{r}}_c(t_{f_1}). \tag{41}$$

Now, substituting (41) into (38), we arrive at

$$\begin{aligned} \mathcal{H}(t_{f_1}) = 1 &+ w_1\|\dot{\boldsymbol{r}}_h(t_{f_1})\|^2 \\ &+ w_2\ddot{\boldsymbol{r}}_h^T(t_{f_1})\big(2\ddot{\boldsymbol{r}}_c(t_{f_1}) - \ddot{\boldsymbol{r}}_h(t_{f_1})\big) = 0. \end{aligned} \tag{42}$$

Finally, computing the final value of the trajectories in terms of the coefficients κ_i from (37), we obtain the following implicit function of t_{f_1}

$$\begin{aligned} \mathcal{H}_1^*(t_{f_1}) = 1 &+ w_1\|\boldsymbol{\kappa}_1\|^2 - 4\frac{w_1}{w_3}\boldsymbol{\kappa}_2^T\boldsymbol{\kappa}_3 \\ &+ 2w_1\sigma\big(\boldsymbol{\kappa}_2^T e^{\sigma t_{f_1}} - \boldsymbol{\kappa}_3^T e^{-\sigma t_{f_1}}\big)\boldsymbol{\kappa}_1 \\ &- 2w_2\sigma^2\big(\boldsymbol{\kappa}_2^T e^{\sigma t_{f_1}} + \boldsymbol{\kappa}_3^T e^{-\sigma t_{f_1}}\big)\ddot{\boldsymbol{r}}_c(t_{f_1}) = 0. \end{aligned} \tag{43}$$

Note that the predicted acceleration, $\ddot{\boldsymbol{r}}_c(t_{f_1})$, as required in (43) can be obtained from the states. To this end, the time derivative of (25) yields

$$\ddot{\boldsymbol{r}}_c = \boldsymbol{R}(\boldsymbol{q}_o)\Big(\boldsymbol{\omega}_o \times (\boldsymbol{\omega}_o \times \boldsymbol{\rho}) + \boldsymbol{\phi}(\boldsymbol{\omega}_o) \times \boldsymbol{\rho}\Big). \tag{44}$$

Therefore, in the pre-capture phase, the optimal trajectory $\boldsymbol{r}_h^*(t)$ and its time derivatives obtained from (37) can be substituted in the control law (14), while the desired orientation trajectories are obtained from $\boldsymbol{\omega}_h^* = \boldsymbol{\omega}_o$. It should be pointed out that since the target satellite has not yet been grasped in this phase, the controller should not take its inertia into account, i.e., one must set $\boldsymbol{M}_o \equiv \mathbf{0}$ and $\boldsymbol{c}_o \equiv \mathbf{0}$ in the controller.

IV. Optimal Maneuvers for Pos-Capture Phase

In the pose-capture phase, we assume that the target satellite and the robot hand have arrived at the interception point with zero relative velocity. Without loss of generality, we assume that the linear velocity of the target satellite is zero, i.e., $\dot{\boldsymbol{r}}_o = \mathbf{0}$. Thus, we can say

$$\boldsymbol{\tau}_h = \boldsymbol{\tau}_o \quad \text{and} \quad \boldsymbol{\omega}_h = \boldsymbol{\omega}_o \qquad \forall t \geq t_{f_1}.$$

The time-optimal control problem being considered here is how to drive the spacecraft from the given initial angular velocity $\boldsymbol{\omega}_o(0)$ to rest in *minimum time* while the Euclidean norm of the torque input is restricted to be below a prescribed value $\tau_{\max}$. To avoid introducing new variables, we keep the same variables J, $\mathcal{H}$, and $\boldsymbol{\lambda}$ that are used in the pervious section. Therefore, the following cost function

$$J = \int_{t_{f_1}}^{t_{f_2}} 1 \; dt$$

is minimized subject to terminal condition $\boldsymbol{\omega}_h(t_{f_2}) = \boldsymbol{\omega}_h(t_{f_2}) = 0$ while the input torque trajectory should satisfy

$$\|\boldsymbol{\tau}_h\| \leq \tau_{\max}. \tag{45}$$

Denoting vector $\boldsymbol{\lambda} \in \mathbb{R}^3$ as the costates, we can write the system Hamiltonian as

$$H = 1 + \boldsymbol{\lambda}^T\boldsymbol{\phi}(\boldsymbol{\omega}_h) + (\boldsymbol{I}_c^{-1}\boldsymbol{\lambda})^T\boldsymbol{\tau}_h. \tag{46}$$

Then, the theory of optimal control [20], [21] dictates that the time-derivative of the costates must satisfy

$$\dot{\boldsymbol{\lambda}} = -\frac{\partial H}{\partial \boldsymbol{\omega}_h} = -\frac{\partial \boldsymbol{\phi}^T}{\partial \boldsymbol{\omega}_h}\boldsymbol{\lambda} \tag{47}$$

where

$$\frac{\partial \boldsymbol{\phi}^T}{\partial \boldsymbol{\omega}_h} = \boldsymbol{I}_c[\boldsymbol{\omega}_h\times]\boldsymbol{I}_c^{-1} - [\boldsymbol{I}_c\boldsymbol{\omega}_h\times]\boldsymbol{I}_c^{-1}, \tag{48}$$

and skew-symmetric matrix $[\boldsymbol{a}\times]$ represents the cross-product, i.e., $[\boldsymbol{a}\times]\boldsymbol{b} = \boldsymbol{a} \times \boldsymbol{b}$. If $\boldsymbol{\tau}_h^*$ is the time-optimal torque history and $\boldsymbol{\omega}_h^*$, $\boldsymbol{\lambda}^*$ represent the solutions of (19) and (47) for $\boldsymbol{\tau}_h = \boldsymbol{\tau}_h^*$ then, according to *Pontryagin's Minimum Principle*, optimal torque $\boldsymbol{\tau}_h^*$ satisfies the equation

$$H(\boldsymbol{\omega}_h^*, \boldsymbol{\lambda}^*, \boldsymbol{\tau}_h^*) \leq H(\boldsymbol{\omega}_h^*, \boldsymbol{\lambda}^*, \boldsymbol{\tau}_h), \quad \forall \boldsymbol{\tau}_h \in \mathbb{R}^3 \ni \|\boldsymbol{\tau}_h\| \leq \tau_{\max} \tag{49}$$

for every $t \in [t_{f_1},\ t_{f_2})$. Equations (46) and (49) together imply that

$$\boldsymbol{\tau}_h^* = -\frac{\boldsymbol{I}_c^{-1}\boldsymbol{\lambda}^*}{\|\boldsymbol{I}_c^{-1}\boldsymbol{\lambda}^*\|}\boldsymbol{\tau}_{\max}. \tag{50}$$

Therefore, the dynamics of the closed-loop system becomes

$$\dot{\boldsymbol{\omega}}_h^* = \boldsymbol{\phi}(\boldsymbol{\omega}_h^*) - \frac{\boldsymbol{I}_c^{-2}\boldsymbol{\lambda}^*}{\left\|\boldsymbol{I}_c^{-1}\boldsymbol{\lambda}^*\right\|}\tau_{\max} \tag{51}$$

The structure of the optimal controller is determined by (47) and (50) together. However, to determine the control input, the initial values of the costates, $\boldsymbol{\lambda}(0)$, should be also obtained. In fact, by choosing different initial values for the costates, we obtain a family of optimal solutions, each of which corresponds to a particular final angular velocity. In general, the two-point boundary value problem for nonlinear systems is challenging. However, as it will be shown in the following, the structure of our particular system (47) and (51) lead to an easy solution when the final velocity is zero. In such a case, it will be shown that the costates and states are related via the following function:

$$\boldsymbol{\lambda}^*(t) = \frac{\boldsymbol{I}_c^2\boldsymbol{\omega}_h^*}{\|\boldsymbol{I}_c\boldsymbol{\omega}_h^*\|\,\tau_{\max}} \qquad \forall t \in [t_{f_1},\ t_{f_2}), \tag{52}$$

despite the fact that the evolutions of the optimal trajectories of the states and costates are governed by two different differential equations (51) and (47). In other words, (52) is a solution to equations (51) and (47). Note that since $\boldsymbol{\omega}_h^*(t) = \boldsymbol{\omega}_h(t) \quad \forall t \in [t_{f_1},\ t_{f_2})$, $\boldsymbol{\omega}_h^*(t_{f_2})$ is not defined, but is assumed nonzero. In such a case, on substitution of (52) into (51), we arrive at the following autonomous system:

$$\dot{\boldsymbol{\omega}}_h^* = \boldsymbol{\phi}(\boldsymbol{\omega}_h^*) - \frac{\boldsymbol{\omega}_h^*}{\|\boldsymbol{I}_c\boldsymbol{\omega}_h^*\|}\tau_{\max} \qquad \forall t \in [t_{f_1},\ t_{f_2}). \tag{53}$$

To prove the above claim, we need to show that (52) and (53) satisfy the optimality condition (47). Using (53) in the time-derivative of right-hand side (RHS) of (52) yields

$$\frac{\mathrm{d}}{\mathrm{d}t}\boldsymbol{\lambda}^* = \frac{\boldsymbol{I}_c^2\boldsymbol{\phi}}{\|\boldsymbol{I}_c\boldsymbol{\omega}_h^*\|\,\tau_{\max}}. \tag{54}$$

On the other hand, using (48) and (52) in the RHS of (47) yields

$$-\frac{\partial\boldsymbol{\phi}^T}{\partial\boldsymbol{\omega}_h}\boldsymbol{\lambda}^* = \frac{\boldsymbol{I}_c^2\boldsymbol{\phi}}{\|\boldsymbol{I}_c\boldsymbol{\omega}_h^*\|\,\tau_{\max}}. \tag{55}$$

A comparison between (54) and (55) clearly proves that (52) is indeed a solution to the differential equation (47). Furthermore, the Hamiltonian on the optimal trajectory becomes

$$H^* = \boldsymbol{\lambda}^{*T}\boldsymbol{\phi}(\boldsymbol{\omega}_h^*) = -\frac{(\boldsymbol{I}_c\boldsymbol{\omega}_h^*)^T[\boldsymbol{\omega}_h^*\times](\boldsymbol{I}_c\boldsymbol{\omega}_h^*)}{\|\boldsymbol{I}_c\boldsymbol{\omega}_h^*\|\,\tau_{\max}} = 0$$

Therefore, the condition for optimality with open end time is also satisfied [21, pp. 213]. Thus, equation (53) generates the optimal angular rate trajectories, and hence the orientation of the robot hand can be obtained from

$$\dot{\boldsymbol{q}}_h^* = \frac{1}{2}\underline{\boldsymbol{\omega}}_h^* \otimes \boldsymbol{q}_h^* \tag{56}$$

Finally, one can use the kinematic relations (25) and (44) to derive the desired trajectories of the translational motion.

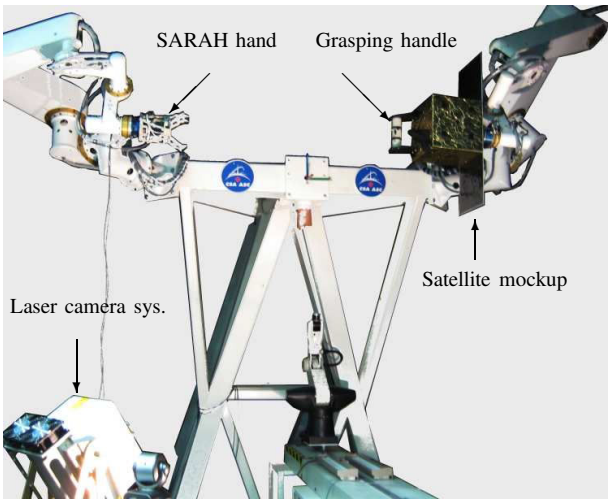

Fig. 2. The experimental setup

V. Simulation and Experimental Results

In this section, experimental results are reported that show the performance of a vision-guided system based on the optimal trajectory descried in Section III for autonomous interception of a tumbling satellite. Fig. 2 illustrates the experimental setup, where two manipulator arms are employed to simulate the motions of the target and the chaser satellites. A mockup of the target satellite is moved by a manipulator according to dynamics of a free-floating rigid body. The other arm, equipped with a robotic hand known as SARAH [22], is used to autonomously approach the mockup and capture its grasping handle. Neptec's laser camera system is used to obtain pose measurements at a rate of 0.5 Hz.

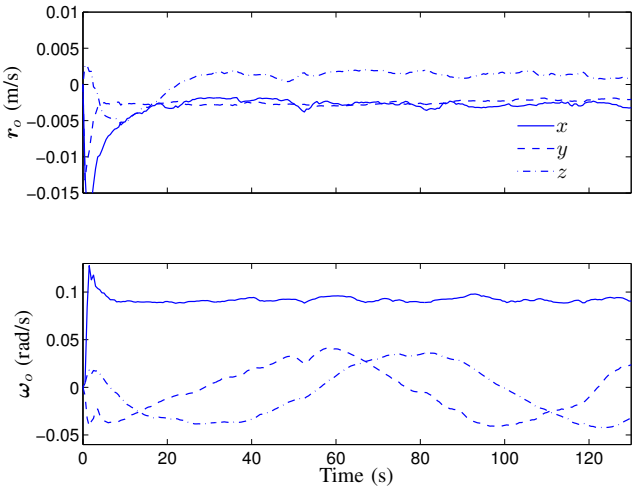

Fig. 3. Estimated translational and angular velocities

The inertia parameters of the target satellite are selected as $I_{xx} = 4$ kgm^2, $I_{yy} = 8$ kgm^2, $I_{yy} = 5$ kgm^2, and $\boldsymbol{\rho} = \mathrm{col}\,(-0.15, 0, 0)$ m. These values are used to determine the manipulator-driven motion of the mockup target. The objective is to capture the grasping handle of the tumbling

mockup smoothly using the robotic arm despite the noisy pose data provided by the laser camera.

During the learning phase, an extended Kalman filer receives the vision data and subsequently estimates the sets of inertial parameters and the states of the tumbling satellite, both of which are required for path planning, see for more details [13], [23].

Figs 3 shows the trajectories of the estimated velocities of the target satellite. Fig. 4 shows the velocity and acceleration trajectories of the grasping handle calculated from the estimated states. Based on these data and the estimated parameters and states at t_0 and weights $1/\sqrt{w_1} = 0.06$ m/s and $1/\sqrt{w_2} = 0.016$ m/s^2, the Hamiltonian is computed from (42). The zero-crossing of the Hamiltonian is then found to occur at $t^*_{f_1} = 148.5$ s; see Fig. 5. Note that $t^*_{f_1}$ corresponds to the optimal interception point. Fig. 6 shows trajectories of the robot end-effector and those of the grasping-handle. It is evident that the robot intercepts the handle at the designated time. Note that the post-grasping operation is not emulated, as both manipulators are stopped upon arriving at the interception point.

Fig. 7 shows the distance between the end-effector and the grasping handle, $\|\boldsymbol{r}_c - \boldsymbol{r}_h\|$, as well as the magnitude of the relative velocity, $\|\dot{\boldsymbol{r}}_c - \dot{\boldsymbol{r}}_h\|$. Apparently, at time $t = t_{f_1}$ both relative distance and velocity vanish.

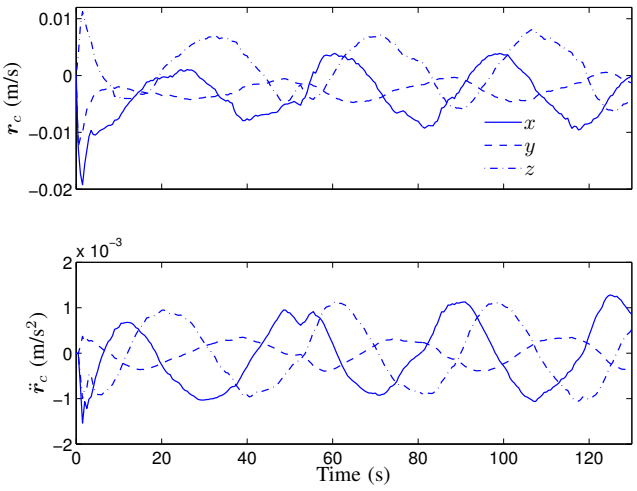

Fig. 4. The velocity and the acceleration of the grasping handle

The detumbling phase of the satellite is demonstrated by simulation. To this end, we assume that the allowable torque

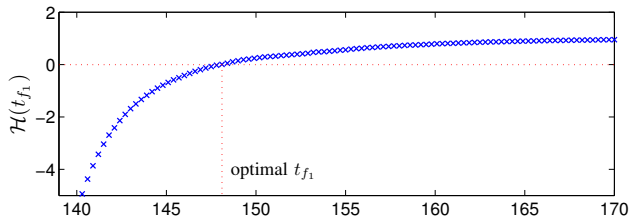

Fig. 5. The Hamiltonian v.s. the terminal time

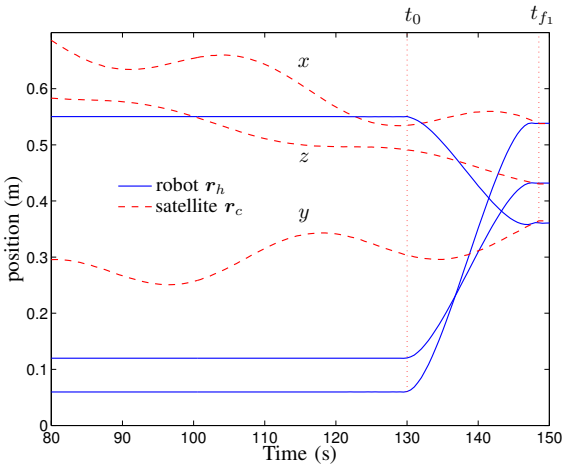

Fig. 6. The trajectories of the satellite and the robot end-effector

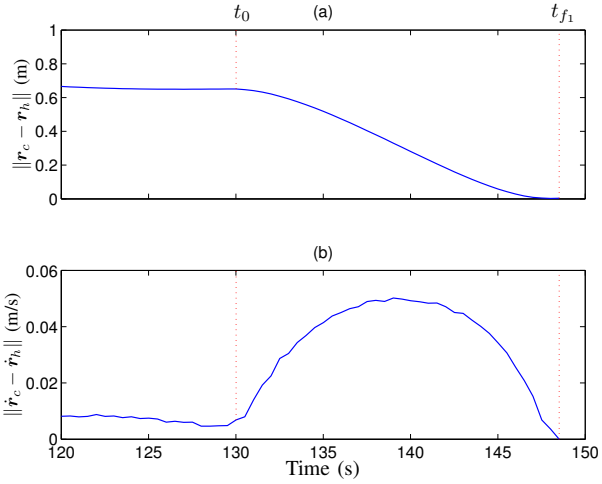

Fig. 7. The Euclidean norms of the relative position and velocity of the satellite with respect to the robot EE

that can be applied to the tumbling satellite is restricted by

$$\|\boldsymbol{\tau}_h\| \leq 0.1 \text{ Nm}, \tag{57}$$

while the spacecraft angular velocity at the instant of capturing is

$$\boldsymbol{\omega}_h(t_{f_1}) = \begin{bmatrix} 0.3 \\ 0.2 \\ 0.1 \end{bmatrix} \text{ (rad/s)}.$$

Fig. 8 illustrates the minimum-time detumbling maneuvers, while trajectories of the optimal torque applied to the satellite is illustrated in Fig. 9.

VI. Conclusions

A method for the guidance of a robotic manipulator to first intercept and then detumble a non-cooperative target satellite has been presented. First, a coordination control for the combined system of the space robot and the target satellite has been developed so that the space robot not only provides the optimal maneuvers dictated by the motion planners but also keeps the attitude of its base undisturbed. Subsequently,

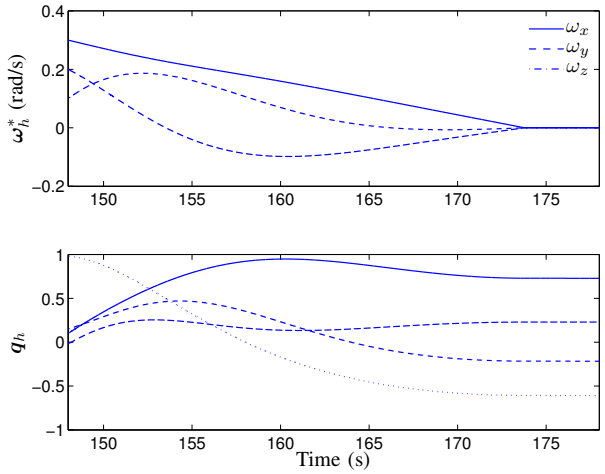

Fig. 8. Optimal detumbling maneuvers.

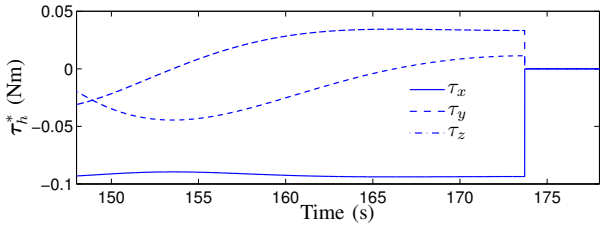

Fig. 9. Trajactories of the torque applied to the tumbling satellite.

two optimal trajectories for the pre-capture and post-capture phases have been developed.

For the pre-capture phase, an optimal intercept trajectory was defined so as to minimize the time of travel along with the weighted norms of the velocity and acceleration of the robot end-effector. The optimization is subject to the constraint that relative-velocity at the rendezvous point becomes zero. For the post-capture phase, i.e., detumbling, a closed-form solution to the time-optimal maneuvers of a spacecraft to bring it to rest subject to the constraint that the magnitude of the torques applied by the robot is below a prescribed value has been found. Finally, experimental results illustrating the autonomous guidance of a robotic manipulator for the capture of a tumbling mockup satellite were reported. In this experiment, another robotic arm was used to move the mockup according to orbital mechanics while a laser vision system was used to obtain pose data. The ability of the detumbling controller was demonstrated by simulation.

REFERENCES

[1] K. Yoshida, "Engineering test satellite VII flight experiment for space robot dynamics and control: Theories on laboratory test beds ten years ago, now in orbit," *The Int. Journal of Robortics Research*, vol. 22, no. 5, pp. 321–335, 2003.

[2] D. Whelan, E. Adler, S. Wilson, and G. Roesler, "Darpa orbital express program: effecting a revolution in space-based systems," in *Small Payloads in Space*, vol. 136, November 2000, pp. 48–56.

[3] G. Hirzinger, K. Landzettel, B. Brunner, M. Fisher, C. Preusche, D. Reintsema, A. Albu-Schaffer, G. Schreiber, and B.-M.Steinmetz, "Dlr's robotics technologuies for on-orbit servicing," *Advanced Robotics*, vol. 18, no. 2, pp. 139–174, 2004.

[4] X. Cyril, A. K. Misra, M. Ingham, and G. Jaar, "Postcapture dynamics of a spacecraft-manipulator-payload system," *AIAA Journal of Guidance, Control, and Dynamics*, vol. 23, no. 1, pp. 95–100, January–February 2000.

[5] D. N. Nenchev and K. Yoshida, "Impact analysis and post-impact motion control issues of a free-floating space robot subject to a force impulse," *IEEE Transactions on Robotics and Automation*, vol. 15, no. 3, pp. 548–557, 1999.

[6] L. B. Wee and M. W. Wlaker, "On the dynamics of contact between space robots and configuration control for impact minimization," *IEEE Transactions on Robotics and Automation*, vol. 9, no. 5, pp. 581–591, October 1993.

[7] G. Faile, D. Counter, and E. J. Bourgeois, "Dynamic passivation of a spinning and tumbling satellite using free-flying teleoperation," in *Proc. of the First National Conference on Remotely Manned Systems*, Passadena, CA, 1973.

[8] B. A. Conway and J. W. Widhalm, "Optimal continuous control for remote orbital capture," *AIAA Journal of Guidance*, vol. 9, no. 2, pp. 149–155, March–April 1986.

[9] S. Matsumoto, Y. Ohkami, Y. Wakabayashi, M. Oda, and H. Uemo, "Satellite capturing strategy using agile orbital servicing vehicle, hyper osv," in *IEEE Int. Conf. on Robotics & Automation*, Washington DC, May 2002, pp. 2309–2314.

[10] A. Ma, O. Ma, and N. Shashikanth, "Optimal control for spacecraft to rendezvous with a tumbling satellite in a close range," in *IEEE/RSJ Int. Conf. on Intelligent Robots and Systems*, Beijing, China, 2002, pp. 4109–4114.

[11] P. Huang, Y. Xu, and B. Liang, "Minimum-torque path planning of space robots using genetic algorithms," *International Journal or Robotics and Automation*, vol. 21, no. 3, pp. 229–236, 2006.

[12] F. Aghili and K. Parsa, "An adaptive kalman filter for motion estimation/prediction of a free-falling space object using laser-vision data with uncertain inertial and noise characteristics," in *AIAA Guidance, Navigation and Control Conference*, Honolulu, Hawaii, August 2008.

[13] ——, "Motion and parameter estimation of space objetcs using laser-vision data," *AIAA Journal of Guidance, Control, and Dynamics*, vol. 32, no. 2, pp. 537–459, March 2009.

[14] D. N. Dimitrov and K. Yoshida, "Momentum distribution in a space manipulator for facilitating the post-impact control," in *IEEE/RSJ International Conference on Intelligent Robots and Systems*, Sendai, Japan, October 2004, pp. 3345–3350.

[15] S. Abiko, R. Lampariello, and G. Hirzinger, "Impedance control for a free-floating robot in the grasping of a tumbling target with parameter uncertainty," in *IEEE/RSJ International Conference on Intelligent Robots and Systems*, Beijing, China, October 2006, pp. 1020–1025.

[16] F. Aghili, "Optimal control of a space manipulator for detumbling of a target satellite," in *IEEE Int. Conference on Robotics & Automation*, Kobe, Japan, May 2009.

[17] J. S.-C. Yuan, "Closed-loop manipulator control using quaternion feedback," *IEEE Transactions on Robotics and Automation*, vol. 4, no. 4, pp. 434–440, August 1988.

[18] J. P. LaSalle, "Some extensions of Lyapunov's second method," *IRE Trans. Circuit Theory*, vol. 7, no. 4, pp. 520–527, 1960.

[19] H. K. Khalil, *Nonlinear Systems*. New-York: Macmillan Publishing Company, 1992, pp. 115–115.

[20] B. D. O. Anderson and J. B. Moore, *Optimal Control*. Englewood Cliffs, NJ: Prince Hall, 1990.

[21] R. F. Stengel, *Optimal Control and Estimation*. New York: Dover Publication, Inc, 1993.

[22] T. Laliberte and C. M. Gosselin, "Underactuation in space robotic hands," in *Proceeding of the Sixth International Symposium on Artificial Intelligence, Robotics and Automation in Space ISAIRAS: A New Space Odyssey*, Montreal, Canada, June 2001.

[23] F. Aghili and K. Parsa, "An adaptive vision system for guidance of a robotic manipulator to capture a tumbling satellite with unknown dynamics," in *IEEE/RSJ Int. Conf. on Intelligent Robots and Systems*, Nice, France, September 2008, pp. 3064–3071.